Geologica Acta, Vol.11, Nº 2, June 2013, 133-148
DOI: 10.1344/105.000001836
Available online at www.geologica-acta.com

geologica acta

Spinel group minerals in metamorphosed ultramafic rocks from Río de Las Tunas belt, Central Andes, Argentina

M.F. GARGIULO [1] **E.A. BJERG** [1] **A. MOGESSIE** [2]

[1] **INGEOSUR (Universidad Nacional del Sur – CONICET)**
San Juan 670, B8000ICN Bahía Blanca, Argentina
Gargiulo E-mail: florenciagargiulo@gmail.com; mfgargiulo@uns.edu.ar
Bjerg E-mail: ebjerg@ingeosur-conicet.gob.ar

[2] **Institut für Erdwissenschaften, Bereich Mineralogie und Petrologie, Karl-Franzens Universität Graz**
Universitätsplatz 2, 8010 Graz, Austria
E-mail: aberra.mogessie@uni-graz.at

ABSTRACT

In the Río de Las Tunas belt, Central Andes of Argentina, spinel group minerals occur in metaperidotites and in reaction zones developed at the boundary between metaperidotite bodies and their country-rocks. They comprise two types: i) Reddish-brown crystals with compositional zonation characterized by a ferritchromite core surrounded by an inner rim of Cr-magnetite and an outer rim of almost pure magnetite. ii) Green crystals chemically homogeneous with spinel (s.s.) and/or pleonaste compositions. The mineral paragenesis Fo+Srp+Cln+Tr+Fe-Chr and Fo+Cln+Tr+Tlc±Ath+Fe-Chr observed in the samples indicate lower and middle grade amphibolite facies metamorphic conditions. Nonetheless, the paragenesis (green)Spl+En+Fo±Di indicates that granulite facies conditions were also reached at a few localities. Cr-magnetite and magnetite rims in zoned reddish-brown crystals and magnetite rims around green-spinel/pleonaste grains are attributed to a later serpentinization process during retrograde metamorphism. The chemical composition of spinel group minerals in the ultramafic reaction zones is determined by the mineral zone where they crystallize. Green pleonaste occurs in the chlorite zone, ferritchromite predominates in the amphibole zone, whereas Cr-magnetite and magnetite are more common in the carbonate zone. The mineral paragenesis of the Río de Las Tunas metaperidotites together with the chemical characteristics of the spinel group minerals support a clockwise P-T path evolution for the ultramafic protoliths during the Paleozoic regional metamorphic cycle of this area.

KEYWORDS | **Spinel group minerals. Metaperidotites. Alpine type belts. Central Andes.**

INTRODUCTION

The Frontal Cordillera tectono-stratigraphical province (Fig. 1A) belongs to the Central Argentinean Andes. It comprises a Neoproterozoic to Middle Cambrian metamorphic basement (Guarguaráz Complex) covered by Upper Carboniferous to Lower Permian marine sedimentary rocks (Alto Tunuyán Formation and equivalent units) intruded by Carboniferous and Permo-Triassic igneous rocks corresponding to the Gondwanic magmatic cycle.

The Guarguaráz Complex (López and Gregori, 2004) comprises three lithological associations: i) the metasedimentary association: schists, gneisses, marls and marbles; ii) the basic subvolcanic-volcanic association: mafic orthoamphibolites and metabasites; iii) the ultrabasic/ultramafic bodies: metaperidotites and serpentinites.

Mafic basic subvolcanic-volcanic associations and ultramafic discontinuous outcrops conform 40km-long NE-SW trending belts, from Del Plata to Del Portillo ranges (33º15' to 33º40' South Latitude; Fig. 1B, C). These sub-parallel belts include metamorphosed ultramafic cumulates, strongly tectonized serpentinites, massive and laminated orthoamphibolites, metabasic dikes and pillow-basalts (Villar, 1975; Villar and Donnari, 1987; Villar and Escayola, 1996; Gregori and Bjerg, 1997; Gargiulo, 2010 and references therein). Some of these mafic and ultramafic bodies are concordant with the metasedimetary suite of the Guarguaráz Complex, while others have been tectonically emplaced through NE trending faults into schists, gneisses, marls or marbles (metasedimentary association).

The whole-rock REE abundances of the Guarguaráz complex mafic rocks (basic subvolcanic-volcanic association) have geochemical signatures ranging from E-MORB (enriched) to N-MORB (normal), while the ultramafics hold REE abundances mainly relative to primitive mantle (Villar, 1996, 1998; Gregori and Bjerg, 1997; López and Gregori, 2004; Gargiulo and Bjerg, 2006; López de Azarevich *et al.*, 2009; Gargiulo, 2010 and references therein). The geochemical and isotopic information available at the moment is not sufficient to define a genetic affiliation between the mafic and ultramafic suites of this complex.

According to several authors (*e.g.* Bjerg *et al.*, 1990; Caminos, 1993; Gregori *et al.*, 1997; Ruviños *et al.*, 1997; López, 2005; Massonne and Calderón, 2008; Gargiulo, 2010; Willner *et al.*, 2011; Gargiulo *et al.*, 2011) the Guarguaráz complex was affected by a clockwise regional metamorphic cycle typical of orogenic terranes. The dominant metamorphic grade of this complex is upper amphibolite facies (644ºC; 9kbar), locally reaching the granulite facies conditions (765ºC; 9kbar).

The available geochronological data for the study area is scarce. Nonetheless, a Rb-Sr isochrone age (500±50Ma) was obtained by Caminos *et al.* (1979) for orthoamphibolites (basic subvolcanic-volcanic association) and mica-schists (metasedimetary association). U-Pb ages (1060-1080Ma) were yielded by Ramos and Basei (1997) on detrital zircons from the metasedimentary association suite of the Guarguaráz complex. López de Azarevich *et al.* (2009) reported a whole-rock Sm-Nd isochrone age (655±76Ma) for the basic subvolcanic-volcanic association suite, but also model ages (1620-990Ma) and εe_{Nd} values (+3.5 - +8.2) indicating a depleted source with Grenville model ages for the mafic rocks. U-Pb ages in the interval 2788-556Ma were obtained by Willner *et al.* (2008) in zircon crystals from the Guarguaráz Complex mica-schists. Maximum abundances restricted to the interval 1420-935Ma indicate that the metasedimentary association of the Guarguaráz Complex is mostly Mesoproterozoic (Grenville). Lu-Hf isotope composition reported by these authors for the mesoproterozoic zircon grains gave $\varepsilon eHf_{(t)}$ (+0.6 - +13.3), suggesting a predominantly juvenile crust in the source area of the metasediments. Zircon crystals with εeHf (-10) belong to those of younger ages (555±8Ma) and they appear to be derived from a recycled mesoproterozoic and/or transamazonian crust. The absence of positive εeHf values after 650Ma seems to indicate that no juvenile crust has been formed afterwards in this area. Willner *et al.* (2008) proposed this youngest juvenile crust formation episode was related with the break-up of the Rodinia supercontinent, which was also mentioned by López de Azarevich *et al.* (2009). Recently, Willner *et al.* (2011) reported Lu-Hf mineral isochrone ages (386-394Ma) (Middle Devonian) for the peak of metamorphism in the metasedimentary association and the basic subvolcanic-volcanic association suites of the Guarguaráz complex. Lower Carboniferous Ar-Ar cooling ages on white mica crystals in metapelites (352.7±0.6Ma; 322.7±2.4Ma) and zircon fission track ages (295±18Ma; 283±19Ma) (Lower Permian) were also reported by these authors, supporting a clockwise P-T path evolution for the metamorphism with a minimum early exhumation rate exceeding 1mm/a.

The Frontal Cordillera mafic-ultramafic belt continues northward up to the Bonilla and Cortaderas ranges (29º S.L.) in the western Precordillera tectono-stratigraphic province (Fig. 1). The Frontal Cordillera and western Precordillera mafic-ultramafic belts were interpreted as an alpine type belt by Villar (1975). Haller and Ramos (1984, 1993) proposed that they integrate a dismembered and metamorphosed ophiolitic complex, the "Famatinian Ophiolite", representing the suture zone due to the accretion of two allochthonous terranes (Cuyania and Chilenia, Ramos *et al.*, 1984, 1986) to western Gondwana during the Lower Paleozoic, giving rise to the Famatinian orogenic cycle of western Gondwana (South America).

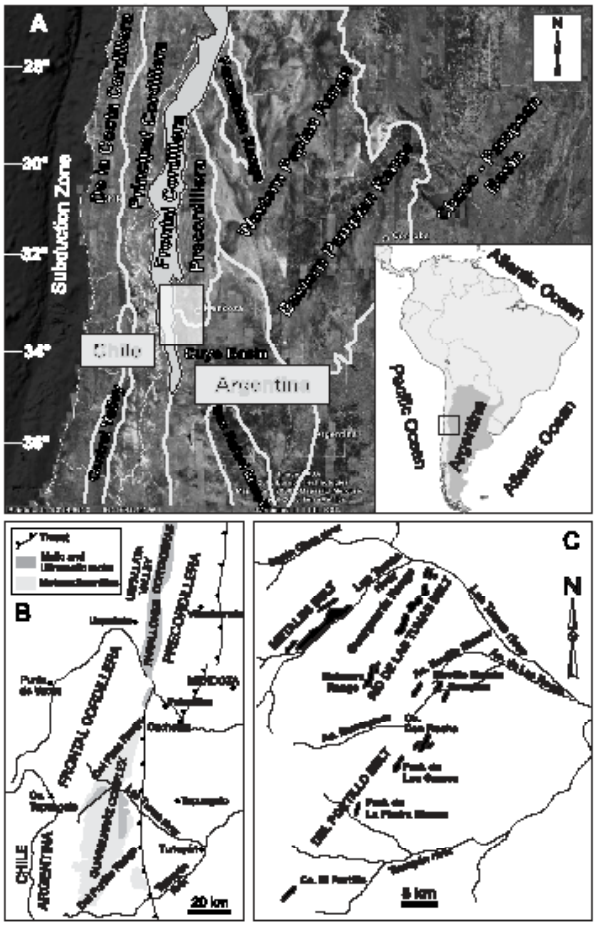

FIGURE 1 | A) Satellite image with the geological configuration of western Argentina and Chile. Tectono-stratigraphical province contours after Ramos (1999). The grey-shaded square represents the area in B. B) Regional sketch-map with the structural relationship between the mafic-ultramafic units in Precordillera and Frontal Cordillera (after Ramos, 2010). C) Sketch-map with the configuration of the Frontal Cordillera Mafic-Ultramafic belts between Del Plata and Del Portillo ranges (modified from Haller and Ramos, 1993; Villar and Escayola, 1996).

Even if there is a good consensus regarding the laurentian affinity of the Cuyania terrain and its accretion to western Gondwana during Ordovician times (Astini *et al.*, 1995; Rapalini and Astini, 1997; Thomas and Astini, 2003 and references therein), the real existence of the Chilenia terrain is still a matter of debate (López and Gregori, 2004; Massone and Calderon, 2008; López de Azarevich *et al.*, 2009; Ramos, 2010; Willner *et al.*, 2011 and references therein). Haller and Ramos (1984) proposed that the hypothetical Chilenia terrain accreted to western Cuyania during the Devonian (Davis *et al.*, 1999, 2000).

The present contribution provides a detailed petrographic and chemical study of the spinel group minerals in metaperidotites from the Río de Las Tunas belt (ultramafic suite of the Guarguaráz complex) and documents the crystallization sequence of the mineral paragenesis observed in these rocks, with the aim to show the importance of the spinel group minerals in the study of the regional metamorphism in ultramafic protoliths.

FIELD RELATIONS OF THE RÍO DE LAS TUNAS BELT

The Río de Las Tunas mafic-ultramafic belt is located on the SE flank of the Guarguaráz range, in the foothills of the Frontal Cordillera (Fig. 1). This belt is comprised by some of the outcrops of the basic subvolcanic-volcanic association and ultramafic suites of the Guarguaráz complex (Fig. 1C).

In the study area (Fig. 2) this complex is intruded by tonalite to granodiorite stocks and diorite dykes related to the Gondwanic magmatic cycle. The studied metaperidotite bodies (ultramafic suite) with NE-SW trend are hosted by or tectonically emplaced into folded NE-striking mica-schists, gneisses, marls and marbles (metasedimentary association suite) or orthoamphiolites (basic subvolcanic-volcanic association unit). The whole sequence has been affected by intense folding, faulting, regional metamorphism and hydrothermal alteration that have almost obliterated the original magmatic nature of the ultramafic rocks. Nonetheless, in some of the outcrops it is possible to recognize relict cumulate textures and primary mineral phases. The ultramafic protoliths reported in this area are: spinel-bearing dunites, clinopyroxene-dunites, wehrlites, olivine-clinopyroxenites and clinopyroxenites (Gargiulo, 2010). Diopsidites, scarce hazburgites and enstatitites were also reported by Villar and Donnari (1987). Dunites and olivine-clinopyroxenites are the most abundant protoliths. At the boundary between ultramafic bodies and their country-rocks it is common to observe reaction zones represented by centimeter-scale roughly concentric and mainly monomineralic concentrations, with gradual transitions between each of them as follows: ultramafic body → talc zone → amphibole zone → chlorite zone → country-rock.

A narrow biotite zone (only a few centimeters wide) can also occur next to the schist or gneiss country-rocks, but where marbles constitute the wall-rock, a massive carbonate zone or magnesite pods are usually present. The size of the entire reaction zone, from the ultramafic body to the country-rock, varies between 1 to 5m wide and seems to be mostly controlled by the size of the ultramafic body itself (Gargiulo, 2010; Gargiulo *et al.*, 2010).

Some of the ultramafic bodies are affected by a 100m-wide shear zone with the same NE regional trend (Fig. 2), where the extreme alteration of the ultramafics gives rise to serpentinites and talc mineralization of economic interest.

ANALYTICAL METHODS

The petrographic study was performed on 252 samples from the study area. Polished thin sections were made from 20 representative samples of the Río de Las Tunas belt. Electron microprobe analyses on mineral phases in the representative samples were carry out using a Jeol SEM 6310 scanning electron microscope at the Institute of Earth Sciences, Mineralogy and Petrology section, Karl-Franzens University of Graz, Austria, using a LINK ISIS energy dispersive system (EDS) and a MICROSPEC wavelength dispersive system (WDS). Routine analyses were set with the following standard conditions: 15kV accelerating voltage and 5nA beam current. Matrix corrections were made using the ZAF procedure. The concentrations of measured elements were calibrated with the following standard minerals: Si, Al, Na, Fe (kaersutite); Mg (olivine); Cr (chromite); Ca, Ti (titanite); Zn (gahnite); Mn (rhodonite); K (adularia); P (apatite); F (F-apatite); Cl (atacamite).

The program NORM 4.0 was used for the atomic proportion calculations of the spinel group mineral formulas. MINPET was used to determine olivine and pyroxene formulae atomic proportions, while for sheet-silicates formulae recalculations the AGT free software templates for Excel worksheets (www.open.ac.uk/earth-research/tindle/AGTWebPages/AGTSoft.html) were used. The amphibole nomenclature and classification were made with the AMPH-CLASS Excel spreadsheet (Esawi, 2004) and checked with the IMA-Amphibole Classification scheme (Mogessie *et al.*, 2004). The program PrismViz (Ganuza *et al.*, 2009) was applied for the spinel group graphical plots and classification diagrams. Mineral abbreviations are those from Kretz (1983).

RÍO DE LAS TUNAS ULTRAMAFIC BODIES

The ultramafic bodies from the study area have been divided in two groups: i) metaperidotites: these comprise the bodies where primary minerals and relict cumulate textures can still be recognized, as well as the metamorphic paragenesis and the established crystallization sequences; ii) serpentinites: these represent extremely altered ultramafic bodies mainly composed by serpentine group minerals and talc, with no preservation of the primary magmatic features.

Metaperidotites

These are black to dark-grey massive bodies, occasionally coarsely foliated. They are often cross-cut by stockwork of fine fibrous serpentine veins (<1mm wide). Most of the metaperidotites preserve relicts of olivine orthocumulates with $spinel_{s.l.}$ as an intercumulus phase (Fig. 3A). Less commonly, intercumulus pyroxene with mesocumulate proportions (Fig. 3B) can also occur. Metaperidotites usually contain between 3 and 5% of disseminated sulphides (mostly pentlandite and pyrrhotite, Fig. 3B), but this amount can reach up to 10% near shear-zones. The primary relict silicates are olivine (Fo_{96-91}) and clinopyroxene (diopside: $En_{50-51}Fs_{01-02}Wo_{49-47}$). The concentration of major elements in the analyzed olivine crystals varies as follows: SiO_2 (42.73-40.48wt%), MgO (54.02-48.95wt%), FeO_{TOTAL} (9.74-3.97wt%), MnO (0.88-0.24wt%), NiO (0.39-0.11wt%), CaO (0.18-0.11wt%). The analyzed clinopyroxene crystals are characterized by the following major element concentrations: SiO_2 (56.22-55.46wt%), CaO (25.28-24.89wt%), MgO (19.53-18.73wt%), FeO_{TOTAL} (0.81-0.67wt%), Cr_2O_3 (0.12-0.10wt%), TiO_2 (0.12-0.10wt%), Al_2O_3 (<0.1wt%), Na_2O (<0.03wt%). The primary silicate phases (olivine and

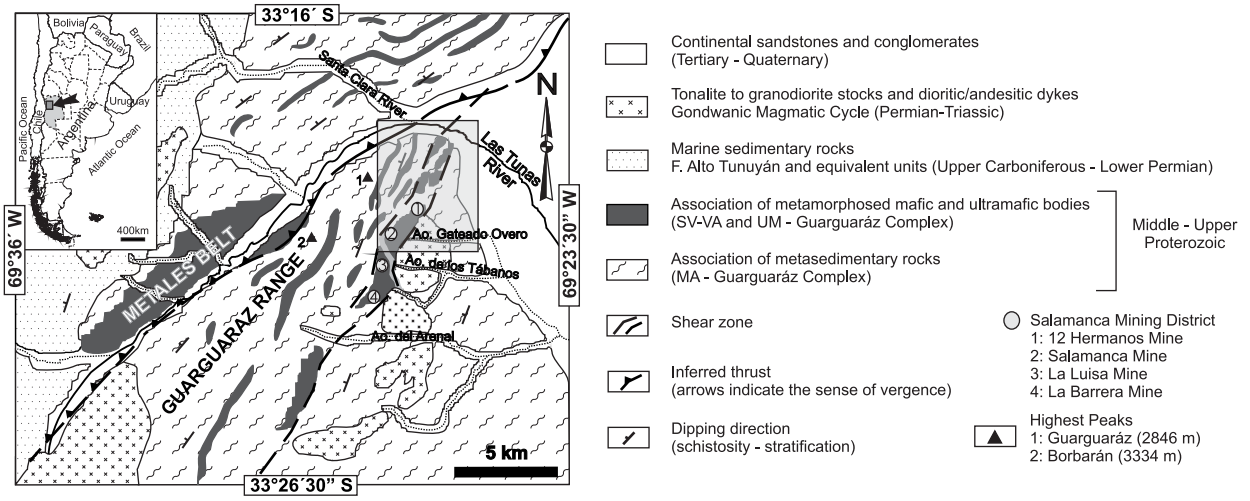

FIGURE 2 | Geological map of the Guarguaráz range, Frontal Cordillera of Argentinean Central Andes (modified from Polanski, 1972; Bjerg *et al.*, 1990). The grey square represents the study area.

pyroxene) are partially replaced by the serpentine group minerals together with brucite and/or chlorite (clinochlore). Talc, amphiboles (mostly tremolite and very locally anthophyllite) and carbonates (dolomite and/or calcite) are also frequent as replacement phases. The main petrographic characteristics of the Río de Las Tunas metaperidotites are listed in Table 1. Representative chemical analyses of chlorite, talc and amphibole are shown in Table I, Electronic Appendix available at www.geologica-acta.com

The mineral paragenesis determined in the Río de Las Tunas ultramafic bodies are the following:

a) $Fo_p \pm Di_p \pm Al\text{-}Chr_p \pm Opx_p$
b) $Fo_p \pm Di_p$ + Srp + Brc + Cln + Mgt
c) Fo_p + Tr ± Tlc + Cln + FeChr + Mgt
d) Fo_p + Ath + Tr ± Tlc ± Cln + FeChr + Mgt
e) Fo_p + Tr ± Tlc ± Cln + Spl/Ple
f) $Fo_p \pm Di_p$ + En + Spl/Ple
Primary relict phases are indicated as a subscript "p".

The crystallization sequences observed in these metaperidotites are summarized as follows:

(1) Primary phases Fo±Di±Al-Chr±Opx → Srp+Mgt(±Brc±Cln). (2) Srp+Mgt (±Brc±Cln) → Tr±Tlc → ±Ath → green Spl+En+Fo±Di. (3) Cln+Tr → Srp+Mgt. (4) Carb (Cal±Dol± Mag).

The crystallization sequence (1) is represented by pseudomorphic serpentinization textures after olivine, orthopyroxene and clinopyroxene, followed by non-pseudomorphic serpentinization textures. Sequence (3) is mostly defined by pseudomorphic serpentinization textures after amphibole and chlorite, non-pseudomorphic and recrystallization serpentinization textures. The carbonate phases (4) developed thereafter, are relatively coetaneous with the generation of the reaction zones between the ultramafics and their country-rocks.

Serpentinites

These are pale-green in color and mostly occur in a 100m-wide shear zone where the alteration of the ultramafic bodies is extreme and the rocks are associated with high proportions of talc (Fig. 4A-D). This shear zone has the same NE general trend as the mafic-ultramafic belt (Fig. 2) and the dominant schistosity of the basement (N20º-80ºE, dipping 50º-80ºNW). The serpentinites show textural evidence of extreme replacement and overprinting processes with several episodes of serpentinization which led to the development of penetrative non-pseudomorphic textures overprinted by a later concentration of talc, occasionally associated with carbonates. The concentration of the major elements in serpentine crystals varies as follows: SiO_2 (46.70-40.19wt%), MgO (46.17-37.71wt%), FeO_{TOTAL} (4.87-1.32wt%), Al_2O_3 (2.35-0.11wt%), Cr_2O_3 (0.80-0.10wt%), NiO (1.37-0.10wt%) and CaO (0.78-0.10wt%). The crystallization sequence observed in these serpentinites is: Srp (non-pseudomorphic) ± Mgt ± Cln → Ctl veins → Tlc ± Carb.

TABLE 1 | Representative petrographic characteristics of Río de Las Tunas ultramafic rocks (Guarguaráz Complex) collected in the shaded area shown in Figure 2

UM rocks from Guarguaráz Complex		Relict primary mineral phases				Metamorphic mineral phases									Observations
Sample	Inferred protolith	Ol	Opx	Cpx	Sulphides / Oxides	Srp	Chl	Tlc	Tr	Ath	Spl	Opx	Carb	Sulphides / Oxides	
24101180 (*)	Unknown	-----	-----	-----	Po, Ag-Pn	x	x	-----	x	-----	-----	-----	-----	Mgt	Serpentinite
131111281(*)	Unknown	-----	-----	-----	-----	x	x	x	-----	-----	-----	-----	-----	Mgt	Serpentinite
12011279	Spinel-Wehrlite	x	-----	x	-----	x	x	x	x	-----	x (**)	-----	x	Mgt	Sm veins
125111281C	Spinel-pyroxene-dunite	x	-----	x	-----	x	x	x	x	-----	x (**)	x	x	Mgt	Ttn, Pmp?, Sericite
158111281	Spinel-dunite	x	-----	-----	Po, Pn, Ccp	x	x	x	x	-----	x (**)	-----	-----	Mgt, Ilm, Mack	Qtz (related to Tr)
17101180	Spinel-dunite	x	-----	-----	Po, Pn, Ccp	x	x	x	x	-----	x	-----	-----	Mgt, Ilm, Vall	Sm veins
7011279	Dunite	x	-----	-----	Ccp	x	x	x	x	-----	-----	-----	x	Mgt	Prh?, Pmp?, Sm
M66D (*)	Unknown	-----	-----	-----	-----	x	-----	x	-----	-----	-----	-----	x	Mgt	Serpentinite
M41	Clinopyroxenite	x	-----	x	Po, Pn, Ccp	x	x	x	x	x	-----	-----	x	Mgt	Carb and Ctl veins
M30A	Wherlite	x	-----	x	Po, Pn, Ccp	x	x	-----	x	-----	-----	-----	x (v)	Mgt	
M32E	Olivine-clinopyroxenite	x	-----	x	Po, Pn	x	x	x	x	x	-----	-----	-----	Mgt	
M37	Olivine-spinel-clinopyroxenite	x	-----	x	Po, Pn	x	x	x	x	-----	x	-----	x	Mgt	
M106D	Clinopyroxene-dunite	x	-----	x	-----	x	x	-----	x	-----	-----	-----	-----	Mgt	
M6	Clinopyroxene-dunite	x	-----	x	Po, Pn, Ccp	x	x	-----	x	-----	-----	-----	-----	Mgt	
M13	Spinel-dunite	x	-----	x	Po, Pn	x	x	x	x	x	x	-----	x	Mgt	
M14	Spinel-dunite	x	-----	-----	Po, Pn	x	x	-----	x	-----	x	-----	x	Mgt	
M52m	Spinel-dunite	x	-----	-----	Pn, Py, Chr	x	x	-----	x	-----	x	-----	x	Mgt	Ctl veins
M93A	Dunite	x	-----	-----	-----	x	x	-----	x	-----	-----	-----	x	Mgt	
M93L	Dunite	x	-----	-----	-----	x	x	-----	x	-----	-----	-----	x	Mgt	
M96	Dunite	x	-----	-----	Pn	x	x	-----	x	-----	-----	-----	x	Mgt	

x: mineral in the sample. (v): mineral in veins. (**) Green crystals. (*) Serpentinites.
Mineral abbreviations from Kretz (1983), except Mack: mackinawite; Vall: vallerite.

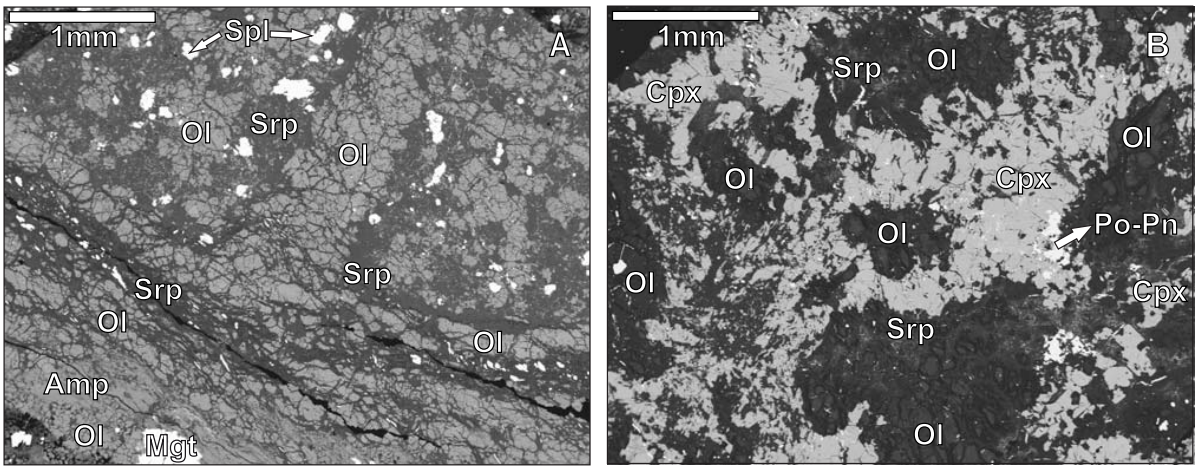

FIGURE 3 | Back scattered electron (BSE) image of metaperidotite with relict olivine orthocumulates and spinel (s.l.) crystals as intercumulus phase. B) Intercumulus pyroxene with mesocumulate proportions. Ol: olivine. Spl: spinel (s.l.). Mgt: magnetite. Srp: serpentine (s.l.). Amp: amphibole (s.l.). Cpx: clinopyroxene. Po: pyrrhotite. Pn: pentlandite.

SPINEL GROUP MINERALS FROM RÍO DE LAS TUNAS METAPERIDOTITES

The highest proportion of spinel group minerals occurs in metaperidotites derived from dunite and pyroxene-dunite protoliths (Table 1). Nevertheless, they also occur in reaction zones developed at the boundary between ultramafic bodies and their country-rocks, mainly in the chlorite and amphibole zones and less commonly in the carbonate zone (Gargiulo, 2010; Gargiulo *et al.*, 2010). $Spinel_{s.l.}$ crystals in dunites and pyroxene-dunites from Río de Las Tunas belt occur as disseminated fine-grained aggregates (20-300μm in size) located interstitially between olivine crystals from the relict cumulate layers or conforming "spinel motes" in the serpentine matrix (Fig. 5A).

Two types of spinel crystals can be distinguished by their color: A) reddish-brown crystals, B) green crystals. Both types always exhibit a dark outer rim of magnetite (Fig. 5B, C). The reddish-brown crystals commonly show compositional zonation (Fig. 5D-G) characterized by a Cr-rich core of ferritchromite (FeChr), surrounded by a Fe-rich rim where the composition grades from Cr-magnetite (CrMgt) to almost pure magnetite (Mgt) at the external rim (Electronic Appendix, Table II). The green crystals are chemically homogeneous with Al-rich compositions ($spinel_{s.s.}$-pleonaste: Spl/Ple) (Fig. 5H, I).

Two crystallization sequences were observed in the spinel group minerals: (1) primary (Al-rich) Chr (rarely preserved) → Fe-Chromite (reddish-brown) → CrMgt → Mgt. (2) Spl/Ple (green) → Mgt.

The spinel group minerals in the ultramafic reaction zones show different textures and compositions depending on the mineral zone where they crystallize. Those in the chlorite zone (Fig. 6A) show two different shapes: i) sub-idiomorphic crystals with sharp contacts with chlorite aggregates or, ii) strongly irregular xenomorphic intergrowths together with chlorite. Both types are green pleonaste crystals (Al-Fe^{2+}-rich compositions) with no significant chemical variations between them. In the amphibole zone (Fig. 6B, C) ferritchromite compositions predominate, whereas Cr-magnetite and magnetite compositions are more common in the carbonate zone. In the latter, spinel group minerals are always present as granular aggregates join together with chlorite and amphibole crystals in thin layers (<900μm) in a calcite groundmass (Fig. 6D, E).

Spinel group minerals chemistry

Spinel group minerals in metaperidotites show a wide range composition: Al_2O_3 (65.71-0.12wt%), TiO_2 (0.74-0.18wt%), #cr (1.000-0.002), #fe (0.991-0.007), #mg (0.766-0.018), MnO (2.51-0.10wt%), ZnO (1.11-0.60wt%). In reaction zones between metaperidotites and their country-rocks the range composition of the spinel group minerals is also wide: Al_2O_3 (54.70-0.27wt%), TiO_2 (1.83-0.11wt%), #cr (0.945-0.033), #fe (0.891-0.062), #mg (0.362-0.000), MnO (0.70-0.27wt%), ZnO (0.82-0.53wt%), but in this case, this variation is relative to the reaction zone in which they crystallize. Representative analyses of spinel group minerals in metaperidotites and reaction zones are shown in Electronic Appendix Table II.

On the basis of the spinel prism (Fig. 7A) for the solid-solution spinel-hercynite-chromite-magnesiochromite-magnesioferrite-magnetite, two chemical variation diagrams (Fig. 7B, C) were constructed with the projections on the triangular face "b" of the spinel prism (Fig. 7A, B) and the compositions on the left-lateral face

"c" of the prism (Fig. 7A, C). These two diagrams have been used to classify the spinel group minerals. Names of middle-member compositions were taken from Haggerty (1991) and Deer *et al*. (1992). The triangular diagram Cr^{3+}-Fe^{3+}-Al^{3+} (Fig. 7B) was modified from Stevens (1944) to fix specific compositional fields for chromite, hercynite and magnetite and other middle-member compositions not considered in the triangular diagram of this author.

Nevertheless, the application of both chemical classification diagrams (Fig. 7B, C) requires caution because they only apply for the solid-solutions mentioned above. This restriction is due to the fact that the contribution of Mn, Zn, Ti and other cations that may be present in the crystalline structure of this mineral group are not considered in these diagrams.

Based on these classification diagrams (Fig. 7B, C) two different compositional groups were identified: i) Al-rich group (hercynite field, Fig. 7B) with a proportion of more than 0.8 of Al as trivalent cation; ii) Cr-Fe^{3+}-rich (Al-poor) group with compositions corresponding to the chromite, ferritchromite, Cr-magnetite and magnetite fields (Fig. 7B), since they have less than 0.2 proportion of Al as trivalent cation.

The ternary diagram (Fig. 7B) shows that relict primary crystals from spinel-metaperidotites belong to the chromite field composition with Al proportions between 0.1 and 0.2. Reddish-brown zoned crystals plot in the transition between ferritchromite and Cr-magnetite fields but also in the magnetite field, with Al proportion below 0.1. On the other hand, green crystals from the spinel-bearing metaperidotites plot in the hercynite field with the highest Al proportion (more than 0.9). The green crystals developed in the chlorite reaction zone also plot in this compositional field with Al proportions higher than 0.8 and Cr mainly below 0.05. Meanwhile those crystals developed in the amphibole zone plot in the ferritchromite field. The crystals from the carbonate zone belong to the Cr-magnetite and magnetite fields with a proportion of Al lower than 0.1.

The binary diagram (Fig. 7C) shows that the Al-rich group compositions plot in the pleonaste and spinel$_{s.s.}$

FIGURE 4 | Field photos of shear zones from Río de Las Tunas belt. A) Contact between metaperidotite and shear zone. B) Juan José Mine: pale-green to white talc-serpentinites in shear zone. C) Detailed field photo showing the complex penetrative non-pseudomorphic texture in serpentinites. D) Talc concentrations in a shear zone. Mineral abbreviations as in Figure 3.

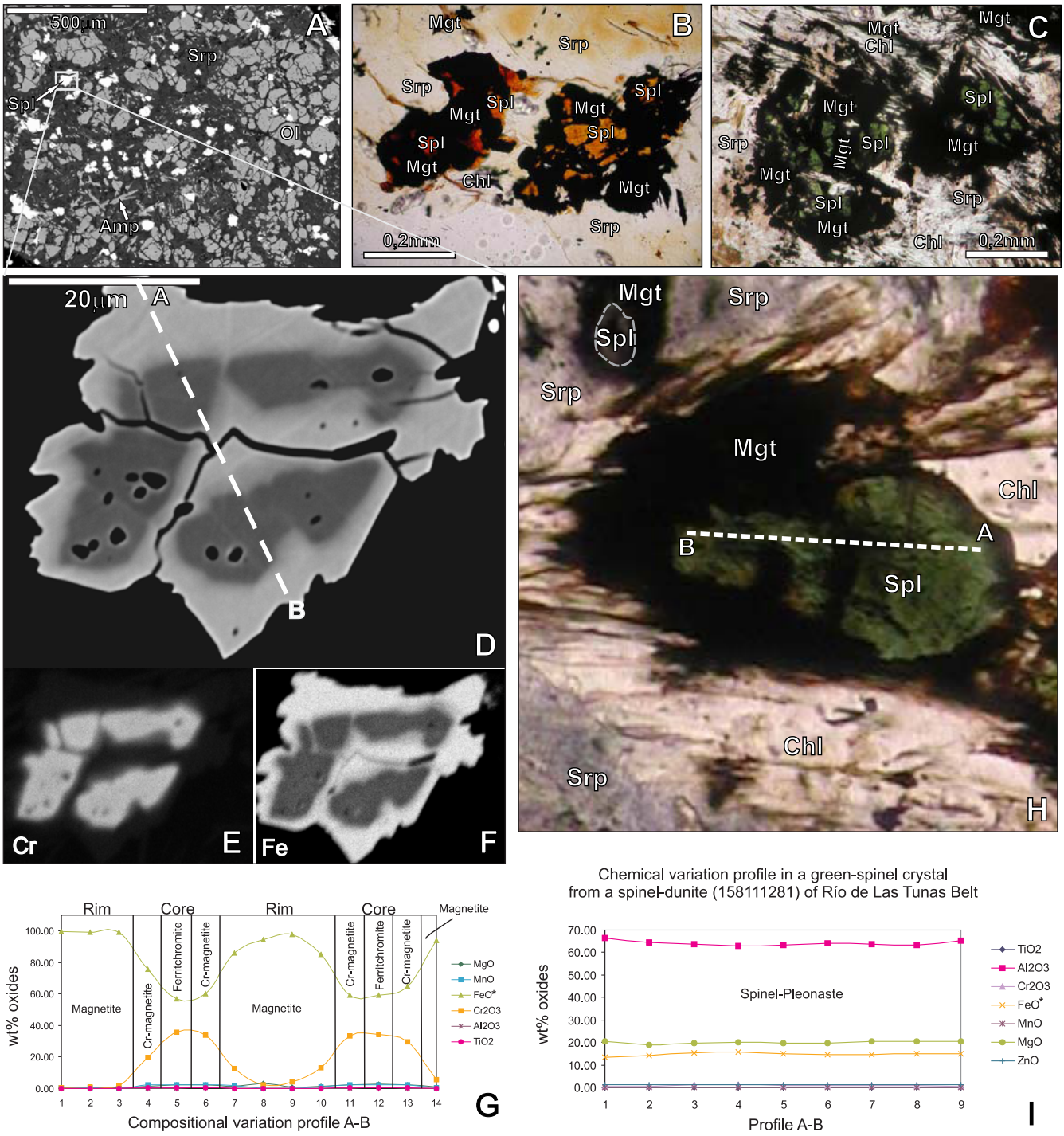

FIGURE 5 | BSE images and photomicrographs of spinel group minerals in metaperidotites from Río de Las Tunas belt. A) BSE image of dunite with spinel s.l. (Spl) granular aggregates (crystals in white) interstitially located between partially serpentinized (Srp) olivine (Ol) cumulus. In the top-left corner a zoned crystal stands out, amplified in D. Near the bottom of the image some acicular aggregates of tremolite amphibole (Amp) replacing serpentine are indicated with a white arrow. B)Photomicrograph (plane-light) of hipidiomorphic to allotromorphic reddish-brown spinels.s. (Spl) crystals partially replaced by magnetite (Mgt) in a serpentine (Srp) and chlorite (Chl) matrix. C) Photomicrograph (plane-light) of allotromorphic green-spinel crystals (Spl) with magnetite (Mgt) rim. D) BSE image of a zoned crystal enclosed in the square in A. Electron microprobe profile was made along line A-B. E) X-ray element (Cr) distribution image of the same crystal shown in Figure 5D. Light-grey color indicates a Cr-rich core. F) X-ray element (Fe) distribution image in the same crystal, with a pale-grey Fe-rich rim. G) Chemical variation profile across the line A-B in the analyzed crystal from A and D showing ferritchromite composition in the core and magnetite composition in the rim. H) Photomicrograph (plane-light) of green-spinel (Spl) crystal. The electron microprobe profile was done along the line A-B. I) Chemical variation profile across the line A-B in the analyzed crystal, showing relatively homogeneous spinel-pleonaste composition along the grain in Figure 5H.

compositional fields. Spinels$_{s.s.}$ from metaperidotites have the highest Mg content (#mg between 0.65 and 0.80), while Al-rich crystals developed in the chlorite zone belong to the pleonaste field only, due to their higher content of Fe^{2+} (#mg between 0.5 and 0.3). The Cr-Fe^{3+}-rich (Al-poor) group shows very low content of Mg (#mg less than 0.2) but some grains with higher proportion of Al and Cr can be distinguished representing the primary relict compositions. The crystals with the highest Fe^{2+} proportion (#mg less than 0.05) are those developed in the carbonate and amphibole zones.

Summarizing, the ternary diagram in Figure 7B is the most suitable for the classification of the chromite-magnetite solid solution middle-members, while the binary diagram (Fig. 7C) is more appropriate for Al-rich middle-members of the spinel-hercynite solid solution, since their compositions do not overlap in the hercynite field as it occurs in the ternary diagram (Fig. 7B).

DISCUSSION

During fractional crystallization of an olivine-chromite-quartz magma system, the olivine is the first mineral to be fractionated from the melt. The composition of the remnant magmatic melt will evolve towards the chromite-olivine cotectic point where both mineral phases will crystallize in equilibrium (Irvine, 1967). If the proportion of chromite is lower than olivine, the chromite grains will be interstitially distributed between the olivine crystals giving rise to dunite cumulates with magmatic chromite intercumulus. The relict cumulate textures preserved in metaperidotites from the Río de Las Tunas belt can be attributed to this process.

The composition of the remnant melt during the crystallization of olivine and chromite phases follows the cotectic curve until it reaches the pyroxene saturation point where pyroxene will crystallize (Irvine, 1967). The presence of Mg-rich clinopyroxene gives rise to the Cr saturation in the system and therefore it is very unusual to have more than 2% of spinel group minerals crystallized in equilibrium with olivine and pyroxene (Barnes and Roeder, 2001). This fact together with the predominance of dunite and clinopyroxene-rich protoliths in the Río de Las Tunas belt (Table 1), allow us to explain why no chromitite pods or chromitite levels were found in this "alpine-type" ultramafic suite, although they are usually present in other orogenic mafic-ultramafic belts around the world.

According to Bjerg *et al.* (1993), relict primary Al-chromite compositions were reported in the core of zoned crystals from the ultramafic bodies of the Metales belt, to the west of the study area (Fig. 2). They reported crystals with an Al-chromite core partially replaced by ferritchromite and Cr-magnetite rims. Nevertheless, they also noted that many analyzed grains from Mina Salamanca, in the Río de Las Tunas belt, comprise instead ferritchromite cores surrounded by Cr-magnetite rims. Therefore they interpreted that most of the primary Al-chromite cores in the ultramafic bodies from the Río de Las Tunas area had been completely replaced by the ferritchromite and Cr-magnetite.

According to Barnes and Roeder (2001 and references therein), the bimodality in nature between chromite and magnetite compositions in many metamorphosed ultramafic rocks is due to the development of metamorphic ferritchromite or magnetite rims on primary magmatic chromite grains. These authors also explain that magnetite and chromite tend to lose Al, in relation to Cr during metamorphism due to reactions with silicates and metamorphic fluids to form chlorite or amphibole. Candia and Gaspar (1997) explain that the formation of clinochlore consumes the MgAl component of the spinels$_{s.l.,}$ while the $Fe^{2+}Fe^{3+}$ component stays as magnetite together with the clinochlore. Chromium enters both magnetite and clinochlore. Therefore, compositions for resulting spinel group minerals usually plot along the Cr-Fe^{3+} join in ternary Cr-Al-Fe^{3+} diagrams like that of Figure 7B, or at the top-right of the diagram in Figure 7C. According to the chemical compositions obtained in the present contribution, two completely different trends are recognized in Figure 7B for the spinel group minerals in metaperidotites of the Río de Las Tunas belt: i) zoned crystals with a ferritchromite to magnetite trend at the Cr-Fe^{3+} join; ii) homogeneous crystals with spinel$_{s.s.}$ or pleonaste compositions restricted to the Al apex.

Bliss and MacLean (1975) attributed the crystallization of secondary ferritchromite or magnetite rims around a primary chromite or spinel grain to the serpentinization process of ultramafic rocks. Barnes and Roeder (2001) consider that zoned crystals generated during regional metamorphism of ultramafic rocks characteristically have Cr-rich cores (where eventually relict magmatic chromite can still be present) and Cr-poor rims displaying a Cr-Fe^{3+} trend in the Cr-Al-Fe^{3+} ternary diagram. This change in the chemical composition of the grains would be the consequence of a recrystallization process during metamorphism mostly at amphibolite facies conditions, with nearly pure magnetite rims developed later during greenschist facies conditions. On the other hand, the Al-rich compositions of spinel crystals from metamorphosed ultramafic rocks are controlled by high-P metamorphic reactions involving silicates like pyroxenes, which also contain Cr-Al-Fe in their crystal structure (Barnes and Roeder, 2001). The composition of these high-grade metamorphic spinels mostly belongs to the spinel-

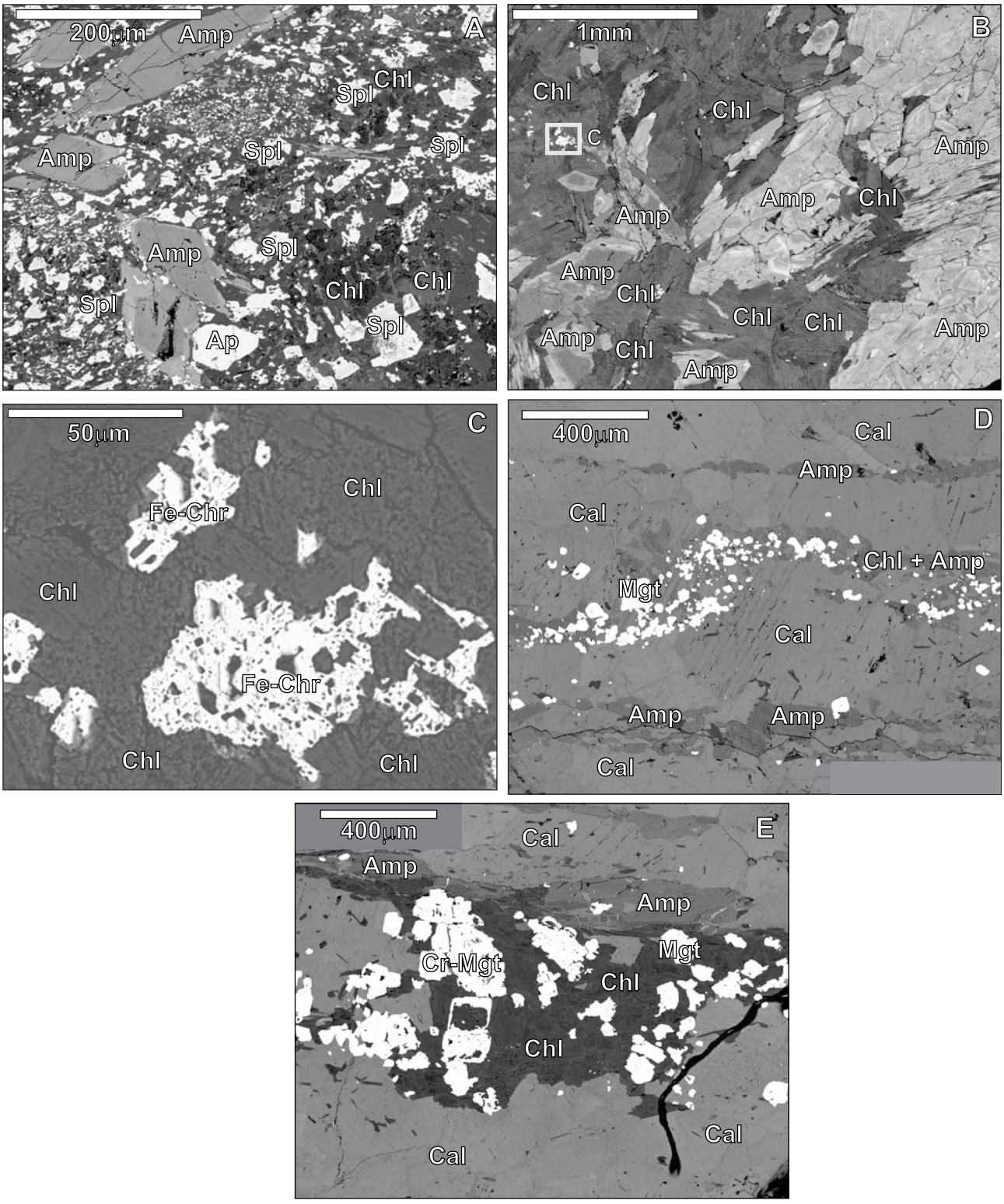

FIGURE 6 | BSE images of samples from reaction zones between metaperidotites and their country-rocks from the Guarguaráz Complex. A) Hipidiomorphic pleonaste (Spl) crystals in sharp contacts with chlorite (Chl) aggregates or strongly irregular xenomorphic intergrowths together with chlorite developed in the chlorite zone, where also amphibole (Amp) and apatite (Ap) may occur. B) Ferritchromite (Chr) crystals from the amphibole zone. C) Magnification from B showing ferritchromite crystals with "corroded" shapes surrounded and partially replaced by chlorite aggregates. D) Chromian-magnetite (Cr-Mgt) and magnetite (Mgt) hipidiomorphic granular aggregates crystallized in carbonate zone related with chlorite and amphibole as fine micro-layers in a calcite (Cal) groundmass. E) Cr-magnetite and magnetite aggregates associated to chlorite and amphibole crystals conforming thin layers in the calcite groundmass.

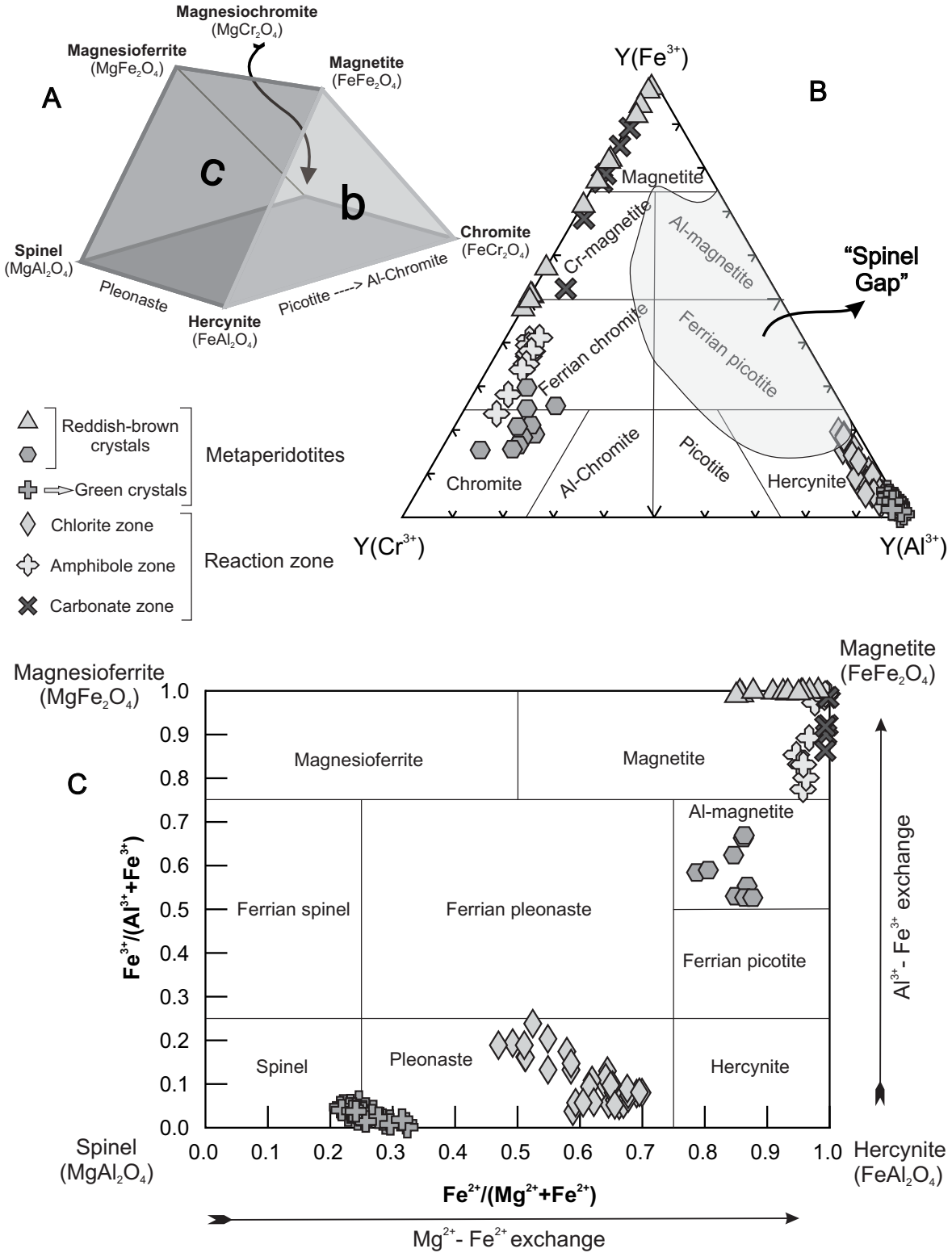

FIGURE 7 | Chemical classification diagrams for the spinel group minerals of Río de Las Tunas belt. A) Spinel prism for the multi-component system: spinel-hercynite-chromite-magnesiochromite-magnesioferrite-magnetite (after Deer *et al.*, 1992). The letter "b" indicated in the triangular-front face and the letter "c" in the lateral-left face of the prism, represent the diagrams in B and C respectively. B) Triangular classification diagram (Cr^{3+}-Fe^{3+}-Al^{3+}): $Y(Cr^{3+})=Cr/(Cr+Fe^{3+}+Al)$; $Y(Fe^{3+})=Fe^{3+}/(Cr+Fe^{3+}+Al)$; $Y(Al^{3+})=Al/(Cr+Fe^{3+}+Al)$. "Spinel gap" field from Barnes and Roeder (2001). C) Binary classification diagram considering the Mg^{2+}-Fe^{2+} exchange in the structural site "X": $Fe^{2+}/(Mg^{2+}+Fe^{2+})$. Field-contours in both diagrams are considering Stevens (1944), Haggerty (1991) and Deer *et al.* (1992).

hercynite series, like the green-spinel/pleonaste crystals in metaperidotite from Río de Las Tunas belt (Fig. 7C). Al-rich green crystals of the spinel-hercynite series, with variable proportions of Fe, Mg and Zn as divalent cations, commonly occur in peridotites affected by regional metamorphism in amphibolite to granulite facies conditions, but they can also crystallize in the black-wall zones associated to these metaperidotites (Frost, 1991), as it is also the case in the Río de Las Tunas belt (Fig. 7C).

According to Evans and Frost (1975) chlorite is the Al-rich mineral phase at lower metamorphic grades. It can be stable up to high grade amphibolite facies conditions but is not preserved under granulite facies conditions because it breaks down to form the Al-rich green-spinel. In this sense, Frost (1991) explains that at high-grade amphibolite facies conditions, after enstatite crystallization and chlorite break-down, spinel group minerals become progressively enriched in Al giving rise to the crystallization of spinel and/or pleonaste. Therefore, the Al released by the chlorite breakdown is fractionated into the spinel crystals displaying Al-rich compositions. Evans and Frost (1975) mentioned that the typical crystallization sequence observed in the spinel group minerals with increasing metamorphic grade is: magnetite →Cr-magnetite → ferritchromite → red-Al-chromite (low Al) → brown-Al-chromite (high Al) → green-spinel, but in metaperidotites of the Río de Las Tunas belt two different crystallization sequences for the spinel group minerals are documented: 1) spinel/pleonaste grains with magnetite rims, 2) Cr-rich zoned crystals with Cr-magnetite to magnetite rims. Both crystallization sequences observed in the studied metaperidotites are formed in the opposite way of the sequence described by Evans and Frost (1975), suggesting a decrease in the P-T conditions during its formation. Thus we attribute these both crystallization sequences to a later serpentinization process during the retrograde stage of the metamorphic cycle.

Another chemical characteristic attributed to $spinel_{s.l.}$ grains crystallized under regional metamorphism by Evans and Frost (1975) is that their compositions plot along the Mg-Fe^{2+} join of the ternary diagram Mg-Fe^{2+}-Zn due to their low content of ZnO. This is also a characteristic shown by the analyzed spinel group minerals from Río de Las Tunas samples (Fig. 8A).

Figure 8B, on the other hand, displays a Fe-Ti trend similar to that attributed to $spinel_{s.l.}$ crystals of magmatic fractional crystallization series. Nonetheless, the compositions represented in this diagram do not belong to such a series since the analyzed crystals were developed in metaperidotites and at the reaction zones with their country-rocks. Barnes and Roeder (2001) interpreted similar trends as the consequence of regional metamorphism affecting spinel-silicate rocks, which is also the case of the analyzed samples.

Figures 7-8 clearly illustrate that analyzed spinel group minerals in metaperidotites from Río de Las Tunas belt have similar chemical characteristics as those described by Evans and Frost (1975) and Barnes and Roeder (2001) for spinel group minerals related to metamorphosed ultramafic rocks from alpine-type complexes.

Mineral paragenesis of metamorphosed ultramafic rocks

Some of the typical mineral paragenesis developed in ultramafic rocks during progressive regional metamorphism are summarized in Table 2. Based on the textural relationships, the mineral paragenesis and the crystallization sequence preserved in metaperidotites from Río de Las Tunas belt (Table 1, see also crystallization sequences in page 137), we interpret sequence (1) as a consequence of a serpentinization process. Sequence (2) evidences a progressive increase in P-T conditions during metamorphism. It is important to note that most of the

TABLE 2 | Typical mineral paragenesis of UM protoliths during progressive regional metamorphism according to Evans and Frost (1975)

Chrysotile/lizardite + brucite + diopside ± chlorite	Prehnite-Pumpellyite facies conditions	
Antigorite + brucite + diopside ± chlorite	Low grade	
Antigorite + olivine + diopside ± chlorite	High grade	Greenschist facies conditions
Antigorite + olivine + tremolite ± chlorite	Low grade	
Talc + olivine + tremolite ± chlorite		
Amphibole (Ca-poor) + olivine + tremolite ± chlorite	Middle grade	Amphibolite facies conditions
Enstatite + olivine + tremolite ± chlorite	High grade	
Enstatite + olivine + tremolite ± green-spinel		
Enstatite + olivine + diopside ± green-spinel	Granulite facies conditions	

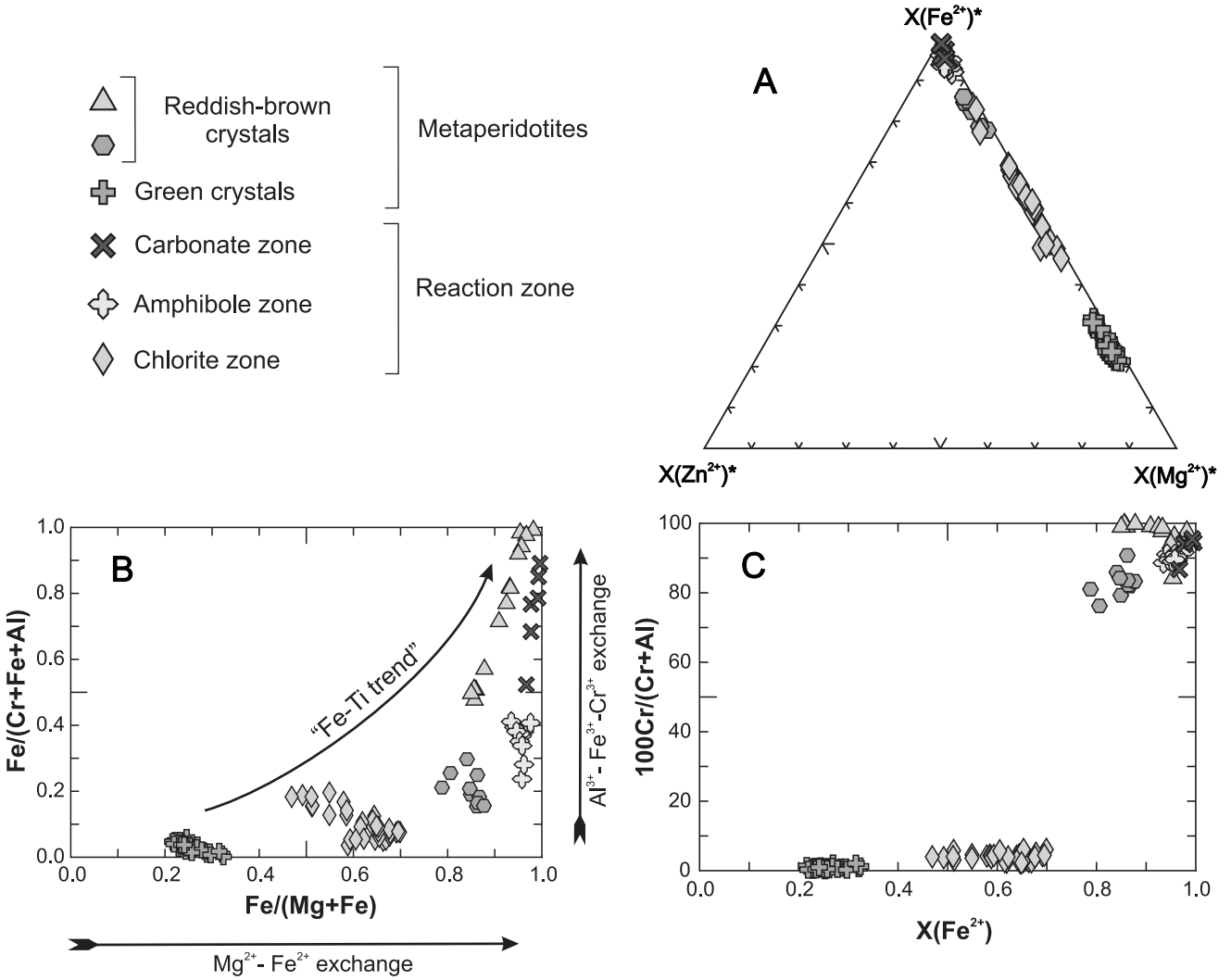

FIGURE 8 | Chemical diagrams for the spinel group minerals of Río de Las Tunas belt. A) Ternary diagram (Zn-Fe^{2+}-Mg) considering these divalent cation proportions in the "X" site of the crystalline structure: $X(Zn^{2+})^*=Zn^{2+}/(Zn^{2+}+Fe^{2+}+Mg^{2+})$; $X(Fe^{2+})^*=Fe^{2+}/(Zn^{2+}+Fe^{2+}+Mg^{2+})$; $X(Mg^{2+})^*=Mg^{2+}/(Zn^{2+}+Fe^{2+}+Mg^{2+})$. See also Table II in the Electronic Appendix. B) Binary diagram with the proportions of $Y(Fe^{3+})$ and $X(Fe^{2+})$ in the crystalline structure: $Y(Fe^{3+})=Fe^{3+}/(Cr+Fe^{3+}+Al)$; $X(Fe^{2+})=Fe^{2+}/(Mg+Fe^{2+})$. The general "Fe-Ti-trend" like path (Barnes and Roeder, 2001) for all the compositions is indicated with a black arrow. C) Binary diagram showing the relationship between the proportion of Cr and Al according to the proportion of Fe^{2+} expressed as: 100Cr/(Cr+Al) and $X(Fe^{2+})=Fe^{2+}/(Mg+Fe^{2+})$. Diagrams after Barnes and Roeder (2001).

samples have tremolite and talc in their parageneses, but anthophyllite is only preserved in a few samples. This means that these rocks have reached at least middle-grade amphibolite facies conditions. Samples where orthopyroxene (Opx) and green-spinel/pleonaste occur together with tremolite represent the transitional conditions to the granulite facies, while the granulite facies was reached only where the paragenesis (green)Spl/Ple+En+Fo±Di is documented in metaperidotites. Sequence (3) represents a drop in the P-T conditions with development of another serpentinization episode after the peak of metamorphism, which is related with the retrograde stage of the metamorphism.

The crystallization of carbonate phases in (4) suggest that a carbonatization process took place after the peak of metamorphism and the serpentinization episode (3), but relatively coetaneous with the development of the reaction zones between the ultramafic bodies and their country-rocks, also during the retrograde stage of the regional metamorphism (Gargiulo *et al.*, 2011). On the other hand, the observed crystallization sequence in serpentinites and talc concentration in shear zones of the study area, are probably genetically related to a later hydrothermal episode mainly located in these shear zones. This episode took place after the emplacement of the igneous bodies of the Gondwanic magmatic cycle in the area (Bjerg, 1985; Gargiulo, 2010; Gargiulo *et al.*, 2011).

CONCLUSIONS

The chemical classification diagrams for the spinel group minerals presented in this contribution allow to

discriminate mineral phases which belong to the spinel-hercynite-chromite-magnesiochromite-magnesioferrite-magnetite series. The ternary diagram (Cr^{3+}-Fe^{3+}-Al^{3+}) is the most suitable for the classification of the Cr-Fe^{3+}-rich middle-members of the chromite-magnetite solid solution, while the binary diagram $Fe^{2+}/(Mg+Fe^{2+})$ *vs*. $Fe^{3+}/(Fe^{3+}+Al)$ is the most appropriate for the Al-rich middle-members of the spinel-hercynite solid solution since their compositions do not overlap in the hercynite field, as it occurs in the ternary diagram (Cr^{3+}-Fe^{3+}-Al^{3+}).

Two compositional groups of $spinel_{s.l.}$ are documented in the metaperidotites of the Río de Las Tunas belt: 1) Cr-Fe^{3+}-rich (Al-poor) group: reddish-brown grains with chemical zonation characterized by ferritchromite core and Cr-magnetite rim grading to almost pure magnetite at the external rim. 2) Al-rich group: green grains chemically homogeneous with $spinel_{s.s.}$ and pleonaste compositions. The Al-rich grains are also surrounded by an external magnetite rim.

The mineral paragenesis and the crystallization sequences observed in the Río de Las Tunas metaperidotites together with the chemical characteristics of the spinel group minerals support a clockwise P-T path evolution for the ultramafic protoliths of the study area during the Paleozoic regional metamorphic cycle. The Al-rich compositions of green spinel/pleonaste grains associated with Fo+En±Di have been controlled by high-P metamorphic reactions. Therefore, this mineral paragenesis represents the highest grade metamorphic condition preserved in the ultramafic unit, indicating that P-T conditions locally reached the granulite facies. The amphibolite facies is the best represented in the study area of the Guarguaráz Complex, where the mineral association Fo_p+Cln+Tr+Tlc+FeChr±Ath indicates that middle grade conditions were reached. Conversely, the more common mineral association Fo_p+Srp+Cln+Tr+FeChr±Tlc indicates that middle to low grade conditions were dominantly preserved. The change in the chemical composition of the reddish-brown zoned grains has been interpreted as the result of recrystallization of Al-chromite primary composition during metamorphism. Fe-chromite was formed mostly at amphibolite facies conditions and the Cr-magnetite to nearly pure magnetite rims were developed later, during greenschist and sub-greenschist facies conditions. The development of magnetite rims around the green-spinel/pleonaste grains also evidence a decrease in the P-T conditions of the system. Thus, the development of Cr-magnetite and magnetite rims in the zoned Cr-Fe^{3+}-rich grains and the magnetite rims on spinel/pleonaste grains are attributed to a later serpentinization process during the retrograde stage of the metamorphism. This is also documented by the pseudomorphic serpentinization textures after amphibole and chlorite and the non-pseudomorphic serpentinization replacements generated afterwards.

In the reaction zones, spinel group minerals show different compositions in each mineral zone where they crystallized. Those in the chlorite zone are green pleonaste with no significant chemical variations. In the amphibole zone ferritchromite compositions predominate whereas Cr-magnetite and magnetite compositions are more common in the carbonate zone. These reaction zones were also developed during the retrograde stage of the regional metamorphism.

ACKNOWLEDGMENTS

The authors are grateful to Dr. S. Delpino from Universidad Nacional del Sur and Dr. G. Ferracutti from INGEOSUR-CONICET-UNS for many helpful discussions and to Ing. L. Ganuza from the VyGLab-UNS for allowing us to use the PrismViz program for the chemical plots of the spinel group minerals. Dr. F. Gallien and Dr. K. Ettinger from Karl-Franzens Universität Graz are also thanked. The authors are grateful to the reviewers of this contribution, Dr. Ibrahim Uysal and Dr. Davide Lenaz, for their useful comments and suggestions which improved our work. Dr. G. Garuti, Dr. F. Zaccarini and the copy-edition team of the Geologica Acta are thanked as well for their kind disposition during the editorial process of the manuscript. Dr. M.F. Gargiulo expresses her gratitude to CONICET of Argentina for Doctoral and Postdoctoral scholarships and to the ÖAD (Austria), for a 6 months scholarship of the North-South Scholarship Program to do research at the Institut für Erdwissenschaften, Bereich Mineralogie und Petrologie, Karl-Franzens Universität Graz. This study was financially supported by CONICET fund projects: PIP. Nro. 6154, PIP. Nro. 112-200801-02306 and by SGCyT-UNS projects: 24/H066, 24/H085, 24/H108 to Dr. E.A. Bjerg.

REFERENCES

Astini, R., Benedetto, J., Vaccari, N., 1995. The early Paleozoic evolution of the Argentina Precordillera as a Laurentian rifted, drifted and collided terrain: a geodynamic model. Geological Society of America, 107 (Bulletin), 253-273.

Barnes, S.J., Roeder, P.L., 2001. The range of spinel compositions in terrestrial mafic and ultramafic rocks. Journal of Petrology, 12, 2279-2302.

Bjerg, E.A., 1985. Aspectos genéticos del proceso de mineralización y su relación con los cuerpos serpentínicos del área de las minas Salamanca, La Luisa y La Barrera, departamento Tupungato, provincia de Mendoza. Doctoral thesis. Universidad Nacional del Sur, Bahía Blanca, Argentina, 93pp.

Bjerg, E.A., Gregori, D.A., Losada Calderón, A., Labadía C.H., 1990. Las metamorfitas del faldeo oriental de la Cuchilla

de Guarguaráz, Cordillera Frontal, Provincia de Mendoza. Revista de la Asociación Geológica Argentina, 45, 234-245.

Bjerg, E.A., Brodtkorb, M.K. de, Stumpfl, E.F., 1993. Compositional zoning in Zn-chromites from the Cordillera Frontal Range, Argentina. Mineralogical Magazine, 57, 131-139.

Bliss, N.W., MacLean, W.H., 1975. The paragenesis of zoned chromites from central Manitoba. Geochimica et Cosmochimica Acta, 39, 973-990.

Caminos, R., 1993. El Basamento Metamórfico Proterozoico-Paleozoico Inferior. In: Ramos, V. (ed.). Geología y Recursos Naturales de Mendoza. 12º Congreso Geológico Argentino y 2º Congreso de Exploración de Hidrocarburos, Mendoza, Argentina. Relatorio 1, 11-19.

Caminos, R., Cordani, U.G., Linares, E., 1979. Geología y geocronología de las rocas metamórficas y eruptivas de la Precordillera y de la Cordillera Frontal de Mendoza, República Argentina. 2º Congreso Geológico Chileno, Arica, Chile. Actas 1, F43-F60.

Candia, M.A.F., Gaspar, J.C., 1997. Chromian spinel in metamorphosed ultramafic rocks from Mangabal I and II complexes, Goiás, Brazil. Mineralogy and Petrology, 60, 27-40.

Davis, J.S., Roeske, S.M., McClelland, W.C., Snee, L.W., 1999. Closing the ocean between the Precordillera terrane and Chilenia: Early Devonian ophiolite emplacement and deformation in the southwest Precordillera. In: Ramos, V.A., Keppie J.D. (eds.). Laurentia-Gondwana connections before Pangea, Colorado, Geological Society of America, 336 (Special Paper), 115-138.

Davis, J.S., Roeske, S.M., McClelland, W.C., Kay, S.M., 2000. Mafic and ultramafic crustal fragments of the southwester Precordillera terrane and their bearing on tectonic models of the early Paleozoic in western Argentina. Geology, 28, 171-174.

Deer, W.A., Howie, R.A., Zussman, J., 1992. An introduction to the rock-forming minerals. Harlow, England, ed. Longman Scientific & Technical, 695pp.

Esawi, E.K., 2004. AMPH-CLASS: An Excel spreadsheet for the classification and nomenclature of amphiboles based on the 1997 recommendations of the International Mineralogical Association. Computers & Geosciences, 30, 753-760.

Evans, B.W., Frost, B.R., 1975. Chrome-spinel in progressive metamorphism – a preliminary analysis. Geochimica et Cosmochimica Acta, 39, 959-972.

Frost, B.R., 1991. Stability of oxide minerals in metamorphic rocks. In: Lindsley, D.H. (ed.). Reviews in Mineralogy. Oxide Minerals: Petrologic and magnetic significance. Vol. 25, Mineralogical Society of America, 469-487.

Ganuza, M.L., Castro, S.M., Martig, S., Ferracutti, G., Bjerg, E., 2009. Mineral compositions visualization implementing the spinel prism. 15º Congreso Argentino de Ciencias de la Computación. Anales, 576-585.

Gargiulo, M.F., 2010. Petrología, geoquímica y evolución metamórfica de la Faja máfica-ultramáfica del Río de Las Tunas, Mendoza, Argentina. Doctoral thesis. Universidad Nacional del Sur, Bahía Blanca, Argentina, 250pp.

Gargiulo, M.F., Bjerg, E.A., 2006. Petrografía y geoquímica de rocas máficas y ultramáficas de Cordillera Frontal, Mendoza. 8º Congreso de Mineralogía y Metalogenia, Buenos Aires, Argentina. Actas, 351-358.

Gargiulo, M.F., Bjerg, E.A., Mogessie, A., 2010. Zonalidad composicional en anfíboles de las zonas de reacción entre los cuerpos ultramáficos y la roca de caja metasedimentaria del Complejo Guarguaráz, Cordillera Frontal de Mendoza, Argentina. 10º Congreso de Mineralogía y Metalogenia, Río Cuarto, Argentina. Actas 1, 85-92.

Gargiulo, M.F., Bjerg, E.A., Mogessie, A., 2011. Caracterización y evolución metamórfica de las rocas ultramáficas de la faja del Río de Las Tunas, Cordillera Frontal del Mendoza. Revista de la Asociación Geológica Argentina, 68, 571-593.

Gregori, D.A., Bjerg, E.A., 1997. New evidence on the nature of the Frontal Cordillera Ophiolitic belt – Argentina. Journal of South American Earth Sciences, 10, 147-155.

Gregori D.A., Ruviños, M.A., Bjerg, E.A., 1997. Las metamorfitas del basamento de la Cordillera Frontal, entre el Río de las Tunas y el Arroyo Barraquero, Provincia de Mendoza. 8º Congreso Geológico Chileno, Antofagasta, Chile. Actas, 2, 857-861.

Haggerty, S.E., 1991. Oxide mineralogy of the upper mantle. Spinel mineral group. In: Lindsley, D.H. (ed.). Reviews in Mineralogy, Oxide minerals: Petrologic and magnetic significance. Vol. 25, Mineralogical Society of America, 355-416.

Haller, M., Ramos, V.A., 1984. Las ofiolitas famatinianas (Eopaleozoico) de las provincias de San Juan y Mendoza. 9º Congreso Geológico Argentino, San Carlos de Bariloche, Argentina. Actas, 2, 66-83.

Haller, M., Ramos, V.A., 1993. Las Ofiolitas y otras rocas afines. In: Ramos, V.A. (ed.). Geología y Recursos Naturales de Mendoza. 12º Congreso Geológico Argentino y 2º Congreso de Exploración de Hidrocarburos, Mendoza, Argentina. Relatorio, 1, 31-39.

Irvine, T.N., 1967. Chromian spinels as a petrogenentic indicator. Part 2 Petrologic applications. Canadian Journal of Earth Sciences, 4, 71-103.

Kretz, R., 1983. Symbols for rock-forming minerals. American Mineralogist, 68, 277-279.

López, V.L., 2005. Geología y Petrología de la Cuchilla de Guarguaráz, Cordillera Frontal de Mendoza. Doctoral thesis. Universidad Nacional del Sur, Bahía Blanca, Argentina, 269pp.

López, V.L., Gregori, D.A., 2004. Provenance and evolution of the Guarguaráz Complex, Cordillera Frontal, Argentina. Gondwana Research, 7, 1197-1208.

López de Azarevich, V.L., Escayola, M., Azarevich, M.B., Pimentel M.M., Tassinari, C., 2009. The Guarguaráz Complex and the Neoproterozoic-Cambrian evolution of the southwestern Gondwana: Geochemical signature and geochronological constrains. Journal of South American Earth Sciences, 28, 333-344.

Massone, H.J., Calderón, M., 2008. P-T evolution of metapelites from the Guarguaráz Complex, Argentina: evidence for Devonian crustal thickening close to the western Gondwana margin. Revista Geológica de Chile, 35, 215-231.

Mogessie, A., Ettinger, K., Leake, B.E., 2004. IMA-Amphibole Classification Scheme, London, Mineralogical Society, www.minersoc.org.

Polanski, J., 1972. Descripción Geológica de la Hoja 24 a-b "Cerro Tupungato", Provincia de Mendoza. Carta Geológico-Económica de la República Argentina, Escala 1:200.000. Boletín 128, Buenos Aires, Dirección Nacional de Geología y Minería de Argentina, 129pp., 1 fold. map.

Ramos, V.A., 1999. Las Provincias Geológicas del Territorio Argentino. In: Caminos, R. (ed.). Geología Argentina. Instituto de Geología y Recursos Minerales, Buenos Aires, Argentina. Anales, 29, 41-96.

Ramos, V.A., 2010. The Grenville-age basement of the Andes. Journal of South American Earth Sciences, 29, 77-91.

Ramos, V.A., Basei, M., 1997. The Basement of Chilenia: an exotic continental terrane to Gondwana during Early Paleozoic. Symposium on Terrane Dynamics´97, New Zealand. Actas, 140-143

Ramos, V., Jordan, T., Allmendinger, R., Kay, S., Cortés, J., Palma, M., 1984. Chilenia: un terreno alóctono en la evolución paleozoica de los Andes Centrales. 9º Congreso Geológico Argentino, San Carlos de Bariloche, Argentina. Actas, 2, 84-106.

Ramos, V., Jordan, T., Allmendinger, R., Mpodozis, C., Kay, S., Cortés, J., Palma, M., 1986. Paleozoic terranes of the central argentine-chilean Andes. Tectonics, 5, 855-888.

Rapalini, A.E., Astini, R.A., 1997. Paleomagnetic confirmation of the Laurentian origin of the Argentine Precordillera. Earth and Planetary Science Letters, 155, 1-14.

Ruviños, M.A., Gregori, D.A., Bjerg, E.A., 1997. Condiciones de P y T del basamento metamórfico de la Cordillera Frontal de Mendoza, Argentina. 8º Congreso Geológico Chileno, Antofagasta, Chile. Actas, 2, 1512-1516.

Stevens, R.E., 1944. Composition of some chromites of the western hemisphere. American Mineralogist, 29, 1-34.

Thomas, W.A., Astini, R.A., 2003. Ordovician accretion of the Argentine Precordillera terrane to Gondwana: a review. Journal of South American Earth Sciences, 16, 67-79.

Villar, M.L., 1975. Las fajas y otras manifestaciones ultrabásicas en la República Argentina y su significado metalogénico. 2º Congreso Iberoamericano de Geología Económica. Actas, 3, 135-155.

Villar, M.L., 1996. Distribución de tierras raras en peridotitas del Complejo Ultramáfico de Novillo Muerto Cordillera Frontal de Mendoza. 3ª Jornadas de Mineralogía, Petrografía y Metalogénesis de Rocas Máficas y Ultramáficas, Publicación del Instituto de Recursos Minerales de la Universidad de La Plata, 5, 327-328.

Villar, M.L., 1998. Los gabros de fondo oceánico de la ofiolita de la Cordillera Frontal de Mendoza, Argentina. 10º Congreso Latinoamericano de Geología y 6º Congreso Nacional de Geología Económica, Buenos Aires, Argentina. Actas, 2, 405-410.

Villar, M.L., Donnari, E.I., 1987. Geología y metalogénesis del Complejo Máfico-Ultramáfico de Los Gateados, Departamento de Tupungato, provincia de Mendoza. 10º Congreso Geológico Argentino, Simposio de Procesos Metalogénicos, Tucumán, Argentina. Correlación Geológica, 3, 45-50.

Villar, M.L., Escayola, M., 1996. Metallogenetic aspects of ophiolites and other types of Mafic and ultramafic complexes of Argentina. In: Coyner, A.R., Fahey, P.L. (eds.). Geology and Ore Deposits of the American Cordillera: Geological Society of Nevada Symposium Proceedings, 1487-1499.

Willner, A.P., Gerdes, A., Massonne, H.J., 2008. History of crustal growth and recycling at the Pacific convergent margin of South America at latitudes 29º-36ºS revealed by U-Pb and Lu-Hf isotope study of detrital zircon from late Paleozoic accretionary systems. Chemical Geology, 253, 114-129.x

Willner, A.P., Gerdes, A., Massonne, H.J., Schmidt, A., Sudo, M., Thomson, S.N. y Vujovich, G. 2011. The geodynamics of collision of a microplate (Chilenia) in Devonian times deduced by the pressure-temperature-time evolution within part of a collisional Belt (Guarguaraz Complex, W-Argentina). Contributions to Mineralogy and Petrology 162, 303-327.

Manuscript received September 2011;
revision accepted May 2012;
published Online January 2013.

ELECTRONIC APPENDIX

TABLE I | Representative electron microprobe analyses of talc (Tlc), chlorites (Chl) and amphiboles (Amp) from the Río de Las Tunas metaperidotites and reaction zones

Sample	Metaperidotites					Chlorite Zone		Amphibole Zone		Carbonates Zone	
Mineral	Tlc			(Chl) Clinochlore		(Chl) Clinochlore		(Chl) Pycnochlorite		(Chl) Pycnochlorite	
SiO_2	59.62	59.21	60.30	31.49	31.05	29.55	29.78	29.29	29.84	29.32	29.44
TiO_2	b.d.l.	b.d.l.	b.d.l.	b.d.l.	b.d.l.	0.14	b.d.l.	b.d.l.	b.d.l.	b.d.l.	b.d.l.
Al_2O_3	0.53	0.60	0.57	16.32	15.63	18.54	18.73	19.01	16.90	17.01	17.19
Cr_2O_3	b.d.l.	b.d.l.	0.29	1.48	3.12	b.d.l.	1.15	0.32	1.44	1.43	0.64
Fe_2O_3	9.27	8.30	8.23	0.00	1.00	0.00	0.69	1.84	0.25	0.00	0.00
MgO	24.17	25.66	24.01	34.51	28.40	27.52	26.15	18.08	25.03	25.06	24.25
MnO	b.d.l.	b.d.l.	b.d.l.	b.d.l.	b.d.l.	0.12	b.d.l.	0.39	b.d.l.	b.d.l.	b.d.l.
FeO	0.00	0.00	0.00	3.78	7.25	11.12	10.33	18.16	13.91	14.27	15.20
NiO	b.d.l.	b.d.l.	b.d.l.	0.13	b.d.l.	b.d.l.	0.56	0.48	b.d.l.	b.d.l.	b.d.l.
ZnO	b.d.l.	b.d.l.	b.d.l.	b.d.l.	b.d.l.	b.d.l.	b.d.l.	b.d.l.	0.12	b.d.l.	b.d.l.
CaO	0.26	0.10	0.15	b.d.l.	b.d.l.	b.d.l.	b.d.l.	0.20	b.d.l.	b.d.l.	0.54
Na_2O	0.14	0.24	0.20	b.d.l.	b.d.l.	b.d.l.	b.d.l.	b.d.l.	b.d.l.	b.d.l.	0.04
K_2O	b.d.l.	b.d.l.	b.d.l.	b.d.l.	b.d.l.	b.d.l.	b.d.l.	b.d.l.	b.d.l.	b.d.l.	b.d.l.
Total	93.98	94.12	93.76	87.71	86.45	86.97	87.40	87.77	87.49	87.09	87.30
O=F,Cl	0.00	0.00	0.00	0.00	0.00	0.00	0.00	0.00	0.00	0.00	0.00
H_2O calc.	4.00	4.00	4.00	12.71	12.22	12.20	12.23	11.74	12.03	11.98	11.95
TOTAL	97.98	98.12	97.76	100.42	98.67	99.17	99.63	99.51	99.52	99.07	99.26
Structural formula based on 22 Oxygen for Tlc and 28 Oxygen for Chl.											
Si	7.835	7.764	7.912	5.914	6.077	5.804	5.827	5.952	5.945	5.865	5.896
Al iv	0.083	0.095	0.088	2.086	1.923	2.196	2.173	2.048	2.055	2.135	2.104
Al vi	0.000	0.000	0.002	1.545	1.692	2.098	2.154	2.529	1.915	1.879	1.959
Ti	--	--	--	--	--	0.020	--	--	--	--	--
Cr	--	--	0.031	0.220	0.483	--	0.178	0.051	0.227	0.227	0.101
Fe^{3+}	0.917	0.819	0.813	0.000	0.147	0.000	0.102	0.282	0.038	0.000	0.000
Fe^{2+}	0.000	0.000	0.000	0.722	1.187	1.846	1.691	3.086	2.317	2.402	2.568
Mn	--	--	--	--	--	0.020	--	0.067	--	--	--
Mg	4.735	5.015	4.696	9.661	8.285	8.058	7.629	5.477	7.433	7.473	7.239
Ni	--	--	--	0.019	--	--	0.089	0.079	--	--	--
Zn	--	--	--	--	--	--	--	--	0.017	0.014	--
Ca	0.037	0.014	0.020	--	--	--	--	0.043	--	--	0.116
Na	0.070	0.121	0.102	--	--	--	--	--	--	--	0.035
K	--	--	--	--	--	--	--	--	--	--	--
F	--	--	--	--	--	--	--	--	--	--	--
Cl	--	--	--	--	--	--	--	--	--	--	--
OH*	4.000	4.000	4.000	16.000	15.997	16.000	16.000	16.000	16.000	15.999	15.992
Sum cat	17.701	17.844	17.677	36.167	35.791	36.042	35.843	35.613	35.947	35.992	36.011

b.d.l.: Content below instrumental detection limit.
Detection limit: 0.1 wt%, except for Na_2O, F, Cl: 0.03 wt%

TABLE I | Continued

Sample	Metaperidotites			Amphibole zone		
AMPH-IMA04	Tremolite	Tremolite	Tremolite	Tremolite	Actinolite	Actinolite
SiO_2	58.36	57.64	59.04	55.81	54.87	55.00
TiO_2	b.d.l.	0.10	b.d.l.	b.d.l.	b.d.l.	b.d.l.
Al_2O_3	0.39	0.97	0.25	1.52	3.06	1.39
Cr_2O_3	0.32	b.d.l.	b.d.l.	0.28	0.60	0.43
MnO	b.d.l.	b.d.l.	0.17	b.d.l.	b.d.l.	b.d.l.
FeO*	1.38	2.49	1.59	7.30	9.78	8.12
ZnO	b.d.l.	b.d.l.	b.d.l.	b.d.l.	b.d.l.	b.d.l.
MgO	24.00	23.07	23.53	19.84	18.19	18.75
CaO	13.12	12.84	13.39	12.36	12.10	12.37
Na_2O	0.09	0.19	0.11	0.35	0.61	0.38
K_2O	0.11	b.d.l.	0.12	0.10	0.16	b.d.l.
NiO	b.d.l.	b.d.l.	b.d.l.	b.d.l.	b.d.l.	b.d.l.
F	b.d.l.	b.d.l.	0.03	b.d.l.	b.d.l.	b.d.l.
Cl	b.d.l.	b.d.l.	0.03	b.d.l.	b.d.l.	b.d.l.
Total	97.77	97.30	98.26	97.56	99.37	96.44
Structural formula based on 23 Oxygen						
Si	7.902	7.860	8.004	7.759	7.569	7.796
ivAl	0.063	0.140	---	0.241	0.431	0.204
Ti	---	---	---	---	---	---
Sum-T	7.965	8.000	8.004	8.000	8.000	8.000
viAl	---	0.015	0.040	0.008	0.066	0.028
Ti	---	0.010	---	---	---	---
Cr	0.034	---	---	0.031	0.065	0.048
Fe^{3+}	0.156	0.284	0.012	0.404	0.529	0.263
Mg	4.810	4.690	4.756	4.112	3.741	3.961
Fe^{2+}	---	---	0.168	0.445	0.599	0.700
Mn	---	---	0.019	---	---	---
Ni	---	---	---	---	---	---
Zn	---	---	---	---	---	---
Sum-C	5.000	5.000	4.996	5.000	5.000	5.000
Mg	0.035	---	---	---	---	---
Fe^{2+}	---	---	---	---	---	---
Mn	---	---	---	---	---	---
Zn	---	---	---	---	---	---
Ni	---	---	---	---	---	---
Ca	1.903	1.875	1.945	1.840	1.787	1.879
Na	0.024	0.050	0.028	0.095	0.162	0.105
Sum-B	1.962	1.925	1.973	1.936	1.950	1.984
Na	---	---	---	---	---	---
K	0.020	---	0.021	0.018	0.028	---
Sum-A	0.020	---	0.021	0.018	0.028	---
Sum (T+C)	12.965	13.000	13.000	13.000	13.000	13.000

b.d.l.: Content below instrumental detection limit.
Detection limit: 0.1 wt%, except for Na_2O, F, Cl: 0.03 wt%

TABLE II | Representative electron microprobe analyses of spinel group minerals from the Río de Las Tunas metaperidotite

Spinel type	Crystals in metaperidotites		Reddish-brown zoned crystals in metaperidotites						Green homogeneous crystals in metaperidotites			
			Core		Rim I		Rim II					
Mineral	Chromite		Ferritchromite		Cr-magnetite		Magnetite		Spinel		Pleonaste	
SiO_2	0.60	0.38	0.47	0.37	0.29	0.34	0.32	0.44	b.d.l.	b.d.l.	b.d.l.	b.d.l.
TiO_2	0.63	0.74	0.66	0.70	0.67	0.56	b.d.l.	b.d.l.	b.d.l.	b.d.l.	b.d.l.	b.d.l.
Al_2O_3	6.73	6.79	0.10	0.25	0.24	b.d.l.	b.d.l.	0.23	64.07	63.57	65.71	64.13
Cr_2O_3	45.49	46.78	35.56	34.33	33.93	29.54	0.61	5.48	0.74	0.66	0.24	0.91
FeO*	38.33	38.29	57.11	59.01	60.36	64.70	99.67	94.17	14.55	14.70	14.32	14.85
MnO	1.78	1.06	2.56	2.24	2.51	2.18	0.31	0.40	b.d.l.	0.10	0.13	b.d.l.
MgO	2.28	2.43	2.48	2.65	2.47	2.15	0.34	0.94	19.50	19.77	18.13	17.93
ZnO	0.90	0.60	n.a	n.a	n.a	n.a	n.a	n.a	1.08	1.11	0.80	1.09
Total	96.74	97.07	98.94	99.55	100.47	99.47	101.25	101.66	99.94	99.91	99.33	98.91
Structural formula based on 3 cations and 4 oxygen												
Cr	1.316	1.344	1.024	0.979	0.959	0.845	0.017	0.153	0.015	0.013	0.005	0.019
Ti	0.017	0.020	0.018	0.019	0.018	0.015	---	---	---	---	---	---
Al	0.290	0.291	0.004	0.011	0.010	---	---	0.010	1.918	1.903	1.981	1.951
Fe^{3+}	0.359	0.324	0.935	0.972	0.995	1.125	1.983	1.838	0.067	0.083	0.015	0.031
ΣTriv (2)	1.983	1.980	1.982	1.981	1.982	1.985	2.000	2.000	2.000	2.000	2.000	2.000
Fe^{2+}	0.814	0.840	0.804	0.808	0.810	0.833	0.973	0.939	0.242	0.229	0.291	0.290
Mn	0.055	0.033	0.079	0.068	0.076	0.067	0.009	0.012	---	0.002	0.003	---
Mg	0.124	0.132	0.135	0.142	0.132	0.116	0.018	0.049	0.738	0.748	0.691	0.689
Zn	0.024	0.016	---	---	---	---	---	---	0.020	0.021	0.015	0.021
ΣDiv (1)	1.017	1.020	1.018	1.019	1.018	1.015	1.000	1.000	1.000	1.001	1.000	1.000
Σcat (3)	3.000	3.000	3.000	3.000	3.000	3.000	3.000	3.000	3.000	3.000	3.000	3.000
$Fe^{3+}/(Fe^{3+}+Fe^{2+})$	0.306	0.279	0.538	0.546	0.551	0.575	0.671	0.662	0.217	0.267	0.048	0.096
$X(Fe^{2+})$	0.867	0.864	0.857	0.850	0.860	0.878	0.982	0.950	0.247	0.234	0.297	0.296
X(Mg) = #mg	0.133	0.136	0.143	0.150	0.140	0.122	0.018	0.050	0.753	0.766	0.703	0.704
X(Mg)*	0.129	0.133	0.143	0.150	0.140	0.122	0.018	0.050	0.738	0.750	0.693	0.689
$X(Fe^{2+})$*	0.846	0.850	0.857	0.850	0.860	0.878	0.982	0.950	0.242	0.229	0.292	0.290
X(Zn)*	0.025	0.016	---	---	---	---	---	---	0.020	0.021	0.015	0.021
Y(Cr)	0.669	0.686	0.521	0.499	0.488	0.429	0.009	0.076	0.007	0.007	0.002	0.009
Y(Al)	0.148	0.148	0.002	0.005	0.005	≈0.000	≈0.000	0.005	0.959	0.952	0.990	0.975
$Y(Fe^{3+})$ = #fe	0.183	0.165	0.476	0.496	0.506	0.571	0.991	0.919	0.034	0.042	0.007	0.015
Cr/(Cr+Al) =#cr	0.819	0.822	0.996	0.989	0.990	≈1.000	≈1.000	0.941	0.008	0.007	0.002	0.009

b.d.l.: Content below instrumental detection limit. Detection limit: 0.1 wt%. n.a.: Element not analyzed.

TABLE II | Cotinued

Spinel type	Reaction Zones									
	Green-spinel in Chlorite Zone				Amphibole Zone				Carbonates Zone	
Classification	Pleonaste				Ferritchromite				Cr-magnetite	Magnetite
SiO_2	0.25	1.20	2.29	0.16	0.50	0.52	1.05	0.54	0.10	b.d.l.
TiO_2	b.d.l.	b.d.l.	b.d.l.	b.d.l.	1.64	1.83	1.44	1.49	0.21	0.11
Al_2O_3	54.38	54.70	50.90	52.67	3.01	2.97	2.99	3.06	0.87	0.27
Cr_2O_3	3.44	2.82	3.26	4.12	36.46	37.03	34.63	46.04	19.97	7.00
FeO*	32.81	32.34	33.71	33.88	55.84	54.67	56.78	46.48	74.10	89.34
MnO	0.44	0.55	0.70	0.62	0.27	0.31	0.31	0.30	0.41	b.d.l.
MgO	7.92	8.01	8.14	7.40	0.72	0.81	1.21	0.78	0.40	b.d.l.
ZnO	0.59	0.68	0.79	0.78	0.53	0.82	0.60	0.79	0.54	b.d.l.
Total	99.83	100.30	99.79	99.63	98.97	98.96	99.01	99.48	96.60	96.72
Structural formula based on 3 cations and 4 oxygen										
Cr	0.076	0.063	0.074	0.092	1.055	1.072	1.002	1.332	0.590	0.206
Ti	---	---	---	---	0.045	0.050	0.040	0.041	0.006	0.003
Al	1.800	1.813	1.730	1.760	0.130	0.128	0.129	0.132	0.038	0.012
Fe^{3+}	0.124	0.123	0.196	0.147	0.725	0.699	0.790	0.454	1.360	1.776
ΣTriv (2)	2.000	1.999	2.000	2.000	1.955	1.950	1.960	1.959	1.994	1.997
Fe^{2+}	0.646	0.638	0.616	0.656	0.983	0.974	0.948	0.968	0.955	1.003
Mn	0.010	0.013	0.017	0.015	0.008	0.010	0.010	0.009	0.013	---
Mg	0.331	0.336	0.350	0.313	0.039	0.044	0.066	0.043	0.023	---
Zn	0.012	0.014	0.017	0.016	0.014	0.022	0.016	0.021	0.015	---
ΣDiv (1)	1.000	1.001	1.000	1.000	1.045	1.050	1.040	1.041	1.006	1.003
Σcat (3)	3.000	3.000	3.000	3.000	3.000	3.000	3.000	3.000	3.000	3.000
$Fe^{3+}/(Fe^{3+}+Fe^{2+})$	0.161	0.162	0.241	0.183	0.425	0.418	0.455	0.319	0.587	0.639
$X(Fe^{2+})$	0.661	0.655	0.638	0.677	0.962	0.957	0.935	0.958	0.977	≈1.000
X(Mg) = #mg	0.339	0.345	0.362	0.323	0.038	0.043	0.065	0.042	0.023	≈0.000
X(Mg)*	0.335	0.340	0.356	0.317	0.038	0.042	0.064	0.041	0.023	≈0.000
$X(Fe^{2+})$*	0.653	0.646	0.627	0.666	0.948	0.936	0.920	0.938	0.962	≈1.000
X(Zn)*	0.012	0.014	0.017	0.017	0.014	0.021	0.016	0.021	0.015	≈0.000
Y(Cr)	0.038	0.031	0.037	0.046	0.552	0.564	0.522	0.694	0.297	0.103
Y(Al)	0.900	0.907	0.865	0.880	0.068	0.067	0.067	0.069	0.019	0.006
$Y(Fe^{3+})$ = #fe	0.062	0.062	0.098	0.074	0.380	0.368	0.411	0.237	0.684	0.891
Cr/(Cr+Al) = #cr	0.041	0.033	0.041	0.050	0.890	0.893	0.886	0.910	0.939	0.946

b.d.l.: Content below instrumental detection limit. Detection limit: 0.1 wt%.